

X-ray crystallographic studies of Pb monolayers on Cu(110) surfaces

S. Brennan

Quantum Metrology Group, National Bureau of Standards, Gaithersburg, Maryland 20899

P. H. Fuoss

AT&T Bell Laboratories, Holmdel, New Jersey 07733

P. Eisenberger

Science Laboratories, Exxon Research and Engineering Company, Annandale, New Jersey 08801

(Received 20 May 1985)

Grazing-incidence x-ray crystallographic studies of Pb monolayers on Cu(110) surfaces have been performed and the unit cells of the commensurate $p(5 \times 1)$ phase and the incommensurate phase have been determined. We find that the commensurate Pb phase forms a unit cell that consists of four Pb atoms and the incommensurate Pb layer has a unit cell of two atoms with a slightly larger near-neighbor spacing. In addition, we find large static displacements perpendicular to the $[\bar{1}\bar{1}0]$ troughs for both phases which may account for some of the unusual two-dimensional melting phenomena observed in this system.

INTRODUCTION

Studies of the order-disorder behavior of Pb monolayers on Cu surfaces have revealed several interesting phenomena. First, low-energy electron diffraction (LEED) studies by Henrion and Rhead (HR) demonstrated that Pb melts at different temperatures on different faces of Cu.¹ On the Cu (110) face HR found a $p(5 \times 1)$ structure with a melting temperature of 325°C. (Bulk Pb melts at 327°C.) On other faces of Cu, Pb formed monolayers with lower melting temperatures: a $c(4 \times 4)$ on the Cu(100) melted at 300°C, a $c(5 \times 1)$ 45° on the Cu(100) melted at 225°C, and a $p(4 \times 4)$ on the Cu(111) melted at 325°C.

This range of melting temperatures prompted a more detailed study of the melting of Pb on the Cu(110) surface by Marra, Fuoss, and Eisenberger (MFE) using grazing-incidence x-ray scattering (GIS).² MFE determined that at least two phases of Pb were formed on the Cu(110) surface: a commensurate phase that melted at $\sim 325^\circ\text{C}$ and an incommensurate phase that melted at 250°C. Their results indicated that the incommensurate Pb phase melted first along the troughs of the Cu(110) surface (at 250°C) and perpendicular to the troughs at a higher temperature ($\sim 325^\circ\text{C}$). In addition, their results suggested a strong interaction between Pb atoms in adjacent troughs. Recently, Fuoss, Brennan, and Eisenberger (FBE) have determined that a range of structures are present as a function of composition and these structures have a continuous range of melting temperatures.³

Although much had been learned about the phase transitions in this system, the detailed nature of the phases present was unknown. HR determined the overall symmetry of the Pb on Cu(110) system to be a $c(2 \times 2)$ structure at low coverages (less than half a monolayer) and a $p(5 \times 1)$ structure at higher coverages (near one monolayer). They proposed a model structure for these phases but did not perform a detailed crystallographic analysis.

MFE interpreted their results in terms of the HR model in spite of their evidence of strong Pb interactions between troughs; an effect not predicted in the HR model.

The present effort is an extension of the MFE work; in deriving the crystallographic unit cells we scanned over 30 Pb diffraction peaks that exist for the two phases using the GIS technique. We find that the unmelted commensurate Pb phase forms a unit cell that consists of four Pb atoms and the melted and resolidified incommensurate Pb layer has a unit cell of two atoms. In addition, we find large static displacements perpendicular to the (110) troughs which account for MFE results. (When discussing the crystal orientations in this paper, we will use the notation that the $[\bar{1}\bar{1}0]$ direction is normal to the surface and the $[110]$ lies in the surface.)

EXPERIMENTAL METHOD

Crystallographic determination of surface structure is very difficult because of the small number of atoms scattering and because of the requirement for surface sensitivity. These difficulties have led to the development of a variety of surface structural probes which interact strongly with the material to give high counting rates and surface sensitivity. Unfortunately, due to this strong interaction, the results of these experiments tend to be hard to interpret. Recently, the use of modern high-brightness x-ray sources, e.g., synchrotron sources, have enabled experimenters to perform x-ray diffraction measurements from monolayers on surfaces.²⁻⁴

The requirements for surface sensitivity and efficient use of the incident photons have dictated the use of a grazing incidence scattering approach. The geometry of these experiments is shown in Fig. 1. The x rays are incident on the sample at a grazing angle ϕ (typically $\sim 0.4^\circ$) and are observed at a second grazing angle ϕ' (typically $\sim 2^\circ$). In this geometry, it is convenient to decom-

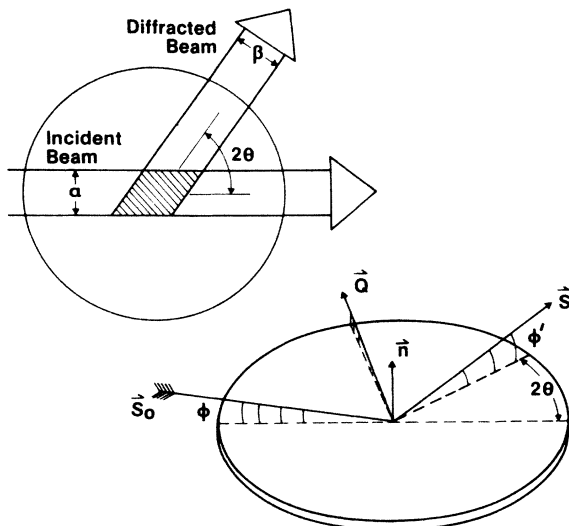


FIG. 1. The grazing incidence scattering geometry showing the incident angle ϕ , the output angle ϕ' , and the scattering angle θ . Also note the area correction given in the inset and described in the data analysis section.

pose the scattering vector (\mathbf{k}) into a component parallel to the surface of the sample and perpendicular to the surface of the sample. The magnitude of the parallel component is given by

$$|\mathbf{k}_{\parallel}| = [2\pi \sin(\theta) / \lambda] [\cos(\phi) + \cos(\phi')], \quad (1a)$$

where θ is one-half the scattering angle projected onto the surface of the sample and λ is the photon wavelength. The magnitude of the perpendicular component is given by

$$|\mathbf{k}_{\perp}| = 2\pi [\sin(\phi) + \sin(\phi')] / \lambda. \quad (1b)$$

For the experiment to be possible surface sensitivity is necessary. The absorption length of Cu $K\alpha$ radiation in Cu is nearly $20 \mu\text{m}$ at normal incidence. Surface sensitivity can be greatly enhanced through the use of refractive index effects, i.e., total reflection of x rays from the surface. At an incidence angle of 0.4° , which is the critical angle for total external reflection, penetration depths of 50 \AA are obtained. The spectra in this experiment were taken with the grazing angle set to the critical angle of the Cu substrate because the electric field intensity at the surface and hence the Pb diffracted intensity is a maximum for that angle. Detailed theories of this process have been presented by Vineyard⁵ and Dietrich and Wagner.⁶

In addition to surface sensitivity, to be successful these experiments require efficient use of the available photons. The grazing incidence mode, at least with present synchrotron radiation sources, results in such use. To understand this, first consider the nature of reciprocal space for a quasi-two-dimensional layer on a surface. As for a bulk material, the two Laue conditions in the plane of the surface result in sharp diffraction peaks in reciprocal space parallel to the surface. However, the Laue condition is relaxed perpendicular to the plane resulting in diffuse

scattering normal to the surface of the sample. Second, synchrotron sources are tightly collimated in the vertical direction but relatively poorly collimated in the horizontal plane. The grazing incidence geometry allows the diffuse scattering direction to be oriented along the poor collimation direction of the synchrotron source resulting in fairly high count rates. This cannot be accomplished in other diffraction geometries and, for example, results in a signal increase of a factor of 50 compared to a transmission experiment.⁷ In addition, under these conditions the polarization vector of the synchrotron radiation is orthogonal to the scattering vector which further enhances the signal rate.

In order to achieve this coupling between reciprocal space and the broad horizontal divergence and polarization properties of synchrotron radiation, the normal to the sample surface must be horizontal. An instrument designed for grazing incidence scattering experiments of phase transitions was used for these studies. This spectrometer, the first of its kind, combines UHV equipment for surface preparation and characterization into the diffractometer itself. The instrument is described in more detail elsewhere.⁴

The experiments were performed at the Stanford Synchrotron Radiation Laboratory under dedicated conditions (3 GeV and 60 mA) on a focused wiggler beamline (BLIV-2) using x rays of wavelength $\lambda = 1.54 \text{ \AA}$. Si(220) monochromator crystals and angular apertures of 1 mrad in the horizontal (perpendicular to the sample surface) and 0.1 mrad vertically defined the incident beam. The diffracted beam was collimated using 1.2 mrad Sollars slits in the plane of the sample surface and 4 mrad perpendicular to the sample surface.

The single crystal of 99.999% Cu was cut and polished such that its surface normal was within 10 mrad of the $[\bar{1}10]$ surface normal. It is difficult to polish the surface of a soft metal without leaving a deep damage layer. The standard treatment is to mechanically polish the surface and electropolish the crystal after having mechanically polished it, which removes the damage layer. Since this step usually destroys the optical figure of the surface, we did not electropolish the Cu surface. Instead, we relied on a very fine mechanical polish ($0.03 \mu\text{m}$) to minimize the damage layer. In the UHV system, repeated argon sputter cycles followed by annealing to 650°C removed the surface sulphur contamination. Residual carbon contamination was removed by annealing at 650°C in 5×10^{-6} -Torr oxygen. Subsequent Auger scans confirmed that the remaining oxygen and carbon contamination was less than 0.01 monolayer.

The sample was dosed with Pb using an evaporator translated to within two inches of the sample. A thermocouple inside the evaporator monitored the Pb temperatures and a shutter was inserted between the evaporator and the crystal to maintain consistent dose times and thus the total dose of Pb on the crystal. HR and MFE reported that monolayer coverages corresponded to a ratio of Auger peaks of approximately 3 to 1 between the Cu peak at 60 eV and the Pb peak at 95 eV; this was used in our work as well. To obtain the commensurate structure the sample was annealed at 300°C for 30 min after deposition.

The incommensurate structure was formed by annealing the commensurate phase at 350°C for 30 min. After annealing an Auger scan was taken to determine whether the surface contamination had increased, but the surface is quite unreactive and no increase in contamination was found.

EXPERIMENTAL RESULTS

After the low-temperature anneal of the as-deposited layer x-ray scattering revealed a monolayer which was ordered and commensurate with respect to the substrate. The dominant diffraction peak coming from the Pb layer was at 1.966 \AA^{-1} which is exactly $\frac{4}{3}$ of the Cu(110) \mathbf{G} (see Fig. 2). Other reflections occurred at 0.4, 1.2, 1.6, and 2.4 times of Cu(110) \mathbf{G} . The strong off-axis reflections were found to be at (0.8,1) (Ref. 8) and (1.6,1) in Cu substrate terms (see Table I). The magnitude of the Cu(001) \mathbf{G} is 1.738 \AA^{-1} . The Pb layer is always in perfect registry along the [001] direction but the diffracted intensity from the (0,1) is considerably weaker than (0.8,0) peak intensity.

After this surface is melted and resolidified the new phase is incommensurate with respect to the substrate structure (see Fig. 2) and is quite stable; the surface layer can be melted and on resolidification returns to the same structure. There are fewer diffraction peaks from this phase than from the high-density phase, the lowest-order reflection now occurring at 1.91 \AA^{-1} which is 0.777 of the Cu(110) \mathbf{G} and thus incommensurate with respect to the substrate (see Table II). We only recorded ten diffraction peaks from the incommensurate phase, which in Cu substrate units are the (0.777,0), (1.54,0), (0,1), (0.777,1), and (1.54,1) and those given by inversion sym-

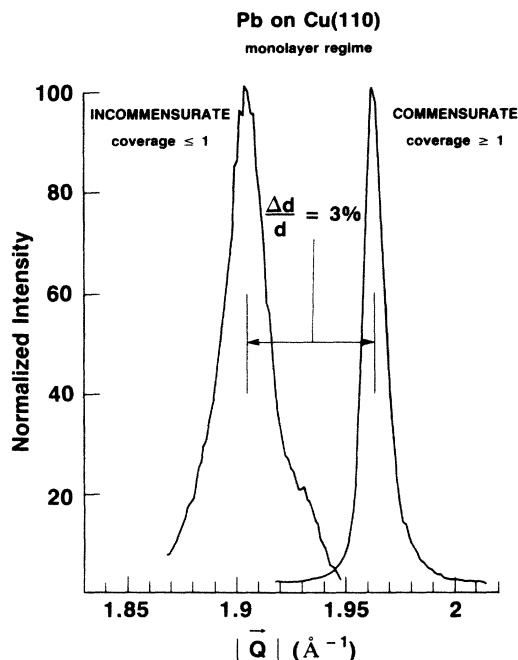


FIG. 2. Representative diffraction peak from the commensurate and incommensurate phases. The commensurate peak is the (0.8,0) reflection and the incommensurate peak is the (0.777,0) reflection.

TABLE I. The diffracted intensities for the commensurate monolayer of Pb on Cu(110). The indices h and k are given as fractions of the Cu(110) and (001) reciprocal-lattice vectors, respectively. The calculated values were obtained using $\bar{u}_{110}=0.12 \text{ \AA}$ and $\bar{u}_{001}=0.17 \text{ \AA}$.

(h,k)	Experimental	Corrected	Calculated
0.2,0	0.000	0.000	0.000
$\bar{0}.4,0$	0.085	0.083	0.006
0.4,0	0.085	0.083	0.006
0.6,0	0.000	0.000	0.000
$\bar{0}.8,0$	6.561	14.380	14.290
0.8,0	6.561	14.380	14.290
1.0,0	0.000	0.000	0.000
$\bar{1}.2,0$	0.012	0.045	0.040
1.2,0	0.021	0.077	0.040
1.4,0	0.000	0.000	0.000
$\bar{1}.6,0$	1.901	9.900	10.190
1.6,0	1.894	9.935	10.190
1.8,0	0.000	0.000	0.000
$\bar{2}.2,0$	0.000	0.000	0.000
2.4,0	0.867	6.188	5.798
0.0,1	1.267	2.394	0.844
0.8,1	0.386	1.213	0.712
1.6,1	0.079	0.458	0.537

metry. During our experiment this structure was very reproducible, but subsequent experiments by FBE have shown that this is one of a range of structures within the incommensurate regime which have varying incommensurability with Pb coverage. This will be discussed in more detail below.

Orthogonal scans along the [110] direction and the [001] direction through the maximum of the diffraction peak were performed to record the scattered intensity. Since these scans sample correlations along the high-symmetry directions, they should provide an accurate representation of the total scattering.

DATA ANALYSIS

We have analyzed our diffraction data by modeling the proposed unit cell and comparing the scattering intensities obtained by this model to the actual scattering intensities. The diffraction peaks were scanned in orthogonal direc-

TABLE II. The diffracted intensities for the incommensurate monolayer of Pb on Cu(110). The indices h and k are given as fractions of the Cu(110) and (001) reciprocal-lattice vectors, respectively. The calculated values were obtained using $\bar{u}_{110}=0.10 \text{ \AA}$ and $\bar{u}_{001}=0.22 \text{ \AA}$.

(h,k)	Experimental	Corrected	Calculated
0.389,0	0.000	0.000	0.000
0.777,0	1.484	3.667	3.718
1.166,0	0.000	0.000	0.000
1.554,0	0.523	3.087	2.988
1.942,0	0.000	0.000	0.000
0.000,1	0.284	0.645	0.499
0.777,1	0.302	1.105	0.552
1.554,1	0.016	0.107	0.446

tions to obtain a representation of the integrated intensity. The integrated intensity was calculated from the data based on the assumption that the shape of a constant intensity cross section through a diffraction peak could be described by an ellipse whose major and minor axes are the widths along the [110] and [001] at that intensity. We did not correct for thermal diffuse scattering from the monolayer but did subtract a constant background which should compensate for the small amount of thermal diffuse scattering from the substrate. The integrated intensities calculated from this algorithm were corrected for three geometric aberrations.

The first correction accounts for the interaction between the finite energy resolution of the monochromator and the diffuse rodlike nature of the x-ray scattering intensity normal to the two-dimensional layer. As pointed out by Marra,⁹ the Ewald spheres defining the minimum and maximum energies transmitted by the monochromator coincide at the origin of reciprocal space. The separation between these spheres is proportional to the photon momentum transfer $|\mathbf{k}|$. For a two-dimensional structure the rod of scattered intensity perpendicular to the layer is long compared to the separation of the Ewald spheres. The scattered intensity is proportional to the intersection of the rod and the Ewald spheres, so the scattering from a two-dimensional (2D) system increases as $\sin(\theta)$. For a three-dimensional crystal the extent of the diffracted intensity in reciprocal space is small compared to the separation between spheres for all nonzero momentum transfers and this correction is unnecessary. For a quasi-two-dimensional structure, the true effect lies between these two extrema. The measured extent of the rods in this experiment is fairly close to the two-dimensional case and much longer than the separation of the Ewald spheres so the data have been multiplied by $1/\sin(\theta)$ to compensate for this effect.

Second, due to the geometry of the scattering (see inset of Fig. 1), the illuminated area (A) of the sample seen by the detector is given by

$$A = \begin{cases} \alpha\beta/\sin(2\theta) & \text{for } \beta/\sin\theta < D, \\ \alpha D & \text{for } \beta/\sin\theta > D, \end{cases} \quad (2a)$$

$$(2b)$$

where α is the height of the incident beam, β is the aperture of the detector, and D is the diameter of the sample. If the area of the sample from which x rays are scattered is small compared to α and β then the term is constant, but for a large area sample the observed volume changes as $\sin(2\theta)$. To correct for this aberration and for the Lorentz factor,¹⁰ the data are multiplied by $\sin^2(2\theta)$. This term is one of the tested parameters in the modeling procedure with the results described below.

Finally, the data must also be compensated for the decrease in the atomic scattering factor with increasing angle. The corrected data (I_c) is related to the measured data (I_m) by

$$I_c = \frac{\sin^2(2\theta)}{\sin(\theta)[(f_0 + f')^2 + (f'')^2]} I_m, \quad (3)$$

where f_0 is the atomic form factor and f' and f'' are the

anomalous scattering factors.¹¹ The values used in this analysis were $f' = -5.0$ and $f'' = 10.0$. The corrected data are given for the commensurate case in Table I and for the incommensurate case in Table II. In addition to the above corrections, the data were multiplied by an overall scale factor to normalize the scattered intensity to that from an individual Pb atom. This factor was empirically determined in the fitting procedure.

After correcting the data for the various aberrations, the scattering was modeled. The starting point for this modeling is the structure factor $S(h,k)$ given by

$$S(h,k) = \sum_{i=1}^N \exp[(2\pi i/\lambda)(hX_i a_1 + kY_i a_2)], \quad (4)$$

where h and k are the Miller indices along the Cu[110] and [001], respectively, N is the number of atoms in the unit cell, λ is the photon wavelength, X_i and Y_i are the fractional coordinates of the i th atom along the Cu[110] and [001] and a_1 and a_2 are the dimensions of the unit cell. Using this $S(h,k)$, the intensity was calculated as

$$I(h,k) = S(h,k) * S(h,k) \exp[-2(k_{110}^2 \bar{u}_{110}^2 + k_{001}^2 \bar{u}_{001}^2)], \quad (5)$$

where k_{110} and k_{001} are the momentum transfers, and \bar{u}_{110} and \bar{u}_{001} are the vibration amplitudes along the Cu[110] and [001], respectively. By systematically varying the set of X, Y values, the vibration amplitudes and an overall scale factor, fits to the data were obtained. The residual used for this fit was defined as

$$\sigma = \sum \frac{|I_c(h,k) - I(h,k)|}{[I_c(h,k)]^{1/2}}, \quad (6)$$

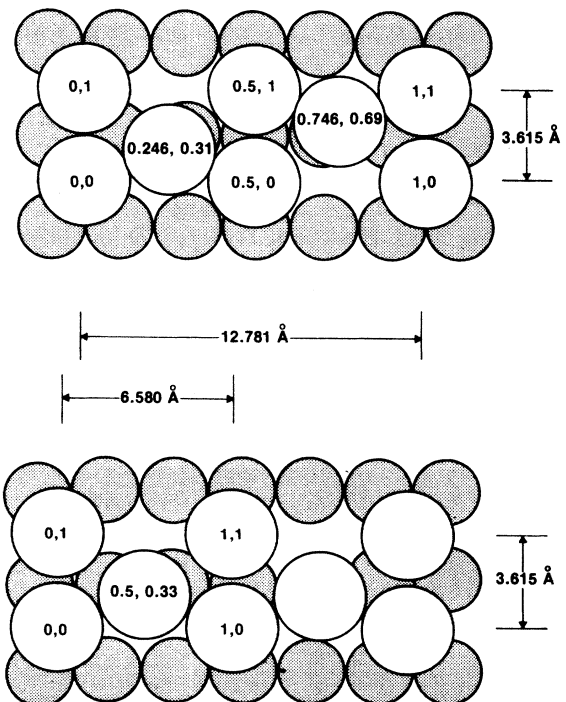


FIG. 3. The calculated structures of (a) the commensurate phase and (b) the incommensurate phase.

where I_c is the observed, corrected data, $I(h,k)$ is the calculated intensity, and the sum runs over the nonzero elements of the data set. Reflections with zero intensity were included by eliminating configurations which resulted in intensities of 0.001 or greater for those reflections.

The final Pb positions for the commensurate phase are shown in Fig. 3(a) along with the first-layer Cu atoms (the shaded circles). The resultant diffracted intensities are tabulated in Table I (under "calculated"). There are four atoms per unit cell (which is 3.615 Å in the [001] direction by 12.781 Å in the [110] direction) at fractional positions of (0,0), (0.246,0.31), (0.5,0), and (0.746,-0.31). The fit included a different vibration amplitude for each direction such that $\bar{u}_{110}=0.12$ Å and $\bar{u}_{001}=0.17$ Å. The residual standard deviation of the 18 peaks involved in this fit was $\sigma=0.13$.

The incommensurate structure has a unit cell of 6.576 Å in the [110] direction [see Fig. 3(b)], is commensurate in the [001] direction and has only two atoms. The atom positions are (0,0) and (0.50,0.33), with $\bar{u}_{110}=0.10$ Å and $\bar{u}_{001}=0.22$ Å. The diffracted intensities are tabulated in Table II. The residual standard deviation for the ten incommensurate reflections was $\sigma=0.22$.

In an effort to determine error limits on these fits, we systematically perturbed the atomic positions and observed the resultant changes in σ . Our model for the commensurate phase has four independent variables, X_2 , Y_2 , \bar{u}_{110} , and \bar{u}_{001} . Since we have collected twelve data points for the commensurate phase, σ must change by 55% for a 90% confidence level in differentiating two structures.¹² Using this criterion, we determined that the atomic positions along the Cu[110] were accurate to ± 0.026 Å and the atomic positions along the [001] were accurate to ± 0.145 Å. The use of asymmetric Debye-Waller factors was not justified by this analysis since the \bar{u}_{001} is not well defined. The error associated with \bar{u}_{110} was ± 0.02 Å.

For the incommensurate phase, the atomic positions were not as well defined because of the limited data set. The allowed deviations along the [110] are very small, < 0.01 Å because of symmetry restrictions and the generally high precision of x-ray scattering measurements. On the other hand, the locations along the [001] direction are very poorly defined. Since for the incommensurate case we had three unknowns and five data points, σ would have to change by 380% for a 90% confidence level. Using that analysis, the atomic position along the [001] could only be determined by $^{+0.43}_{-0.18}$ Å. This lack of definition is partly due to the large discrepancy on the (0.777,1) reflection and our inability to find a model which fits that peak. It is interesting to note that the Pb-Pb distance is 3.50 Å (the bulk Pb-Pb distance) in the derived structure and that σ rapidly increases if Y is reduced below 0.33. The Debye-Waller factors for the incommensurate phase are only determined to ± 0.1 Å.

DISCUSSION

The best way to visualize the unit cell is by considering the Pb atoms as forming rumpled dimers, similar to the situation of thallium on Cu(100) surfaces.¹³ If the Pb

atoms are equally spaced in the [110] direction then the lowest-order diffraction peak is the (0.8,0) reflection. By dimerizing the atoms, pulling the second and fourth atoms off the symmetric positions at 0.25 and 0.75 of a unit cell the reflection at (0.4,0) arises. The y components of the second and fourth atoms is a way of reducing the strain energy of the chains of Pb atoms along the [110] direction. The very weak (0,1) peak is due to the zig-zag Pb chains. The rumpling of the rows of Pb atoms reduces the intensity of that peak from that comparable to the (0.8,0) peak by 4 orders of magnitude due to interference terms. If rumpling were not present, the distance between Pb neighbors would be 3.195 Å. With rumpling, the distance increases to 3.386 Å, still less than the bulk-Pb distance of 3.500 Å. The addition of dimerization indicated by our data creates two Pb-Pb distances, 3.338 and 3.434 Å. As depicted in Fig. 3(b) the rumpled Pb dimers form a zig-zag pattern, i.e., the displacement of the fourth atom in the y direction is opposite to that of the second atom. Our data clearly supports this model relative to a model where the fourth atom y displacement is the same direction as that of the second.

There is one alternate model which does not make use of the dimer model which would fit the available data. If the second and third atoms were lifted off the surface plane by 0.8 Å the Pb-Pb near neighbor distance would be constant at 3.434 Å. The present data is not sensitive to displacements normal to the surface because the profile of the rod intensities were not measured. However, we do not believe this model is likely because the z component would be extremely large.

The LEED pattern exhibited by this surface is a $p(5 \times 1)$ structure which indicates that the repeat distance is four Pb atoms for every five Cu atoms. Our data do not include peaks at (0.2,0) and (0.6,0) which the LEED pattern shows, but this can be explained as being due to multiple scattering of the electrons from the surface, which allows translations by reciprocal-lattice vectors. Thus the peak at (1.2,0) would in the LEED data also be visible at (0.2,0) and the peak at (1.6,0) would be seen at (0.6,0).

As discussed above, one of the parameters that must be tested in the analysis procedure is whether the Cu substrate domain size is large or small compared to the area illuminated by x rays. If the domain size is larger the data should include a correction factor in $\sin(2\theta)$, otherwise this term is replaced by a constant. For a perfect single-crystal surface the correction factor is added, but for a surface that is twinned or includes low-angle grain boundaries the constant factor may be correct. After the final model was determined this additional $\sin(2\theta)$ was removed to compare the goodness of fit without this term. The results are quite clear, the best fit without the additional $\sin(2\theta)$ term has a residual which is over twice as large ($\sigma=0.26$) as with the geometrical correction factor. There is very little difference in the atomic positions with and without the factor, the major change is in the Debye-Waller term along the [110] direction which increases from 0.12 to 0.19 Å. From the fit of the data we concluded that in this case the $\sin(2\theta)$ term was necessary, however this may not be true for every sample that is in-

vestigated. The term will have to be experimentally tested in each case.

Several aspects of the analysis should be emphasized. The first is that the data fit is as dependent on the lack of scattering from certain peaks as it is on the actual value of the scattering intensity from others. Where this effect is strongest is in the requiring that the separation of the first and third atoms ($0.5a_1$) be the same as the separation of the second and fourth atoms. If the 2–4 separation is changed by as little as 0.005 Å, the calculated intensity from missing reflections such as (0.2,0), (0.6,0), and (1.4,0) G increase in strength by 4–5 orders of magnitude.

The vibration amplitudes \bar{u}_{110} and \bar{u}_{001} were optimized in the fitting procedure and the “best-fit” values are lower than those expected for bulk Pb. Reference 11 lists $\bar{u}_x = 0.206$ Å for Pb whereas we find that $\bar{u}_{110} = 0.12$ Å for the commensurate layer and $\bar{u}_{110} = 0.10$ Å for the incommensurate phase. Considering that the derived values are for a Pb monolayer on the surface these values are quite reasonable. In both the commensurate and incommensurate layers the Pb-Pb distance along the [110] direction is smaller than in bulk Pb whereas the distance between Pb atoms in the [001] direction is slightly larger. Since repulsive potentials tend to be much harder than attractive potentials, the observed difference in surface vibrational amplitude is consistent with our derived structure.

The model of the incommensurate phase is a direct extension of the commensurate model with a slightly expanded unit-cell dimension and the centered atom moving into the symmetry position at (0.33,0.5). The registry of both of these unit cells with respect to the substrate is open to question, and the position shown in Fig. 3 are based on the assumption that the Pb atoms will settle into

a Cu fourfold hollow site whenever possible and will always lie in the troughs along the [110].

CONCLUSIONS

Other studies of Pb on Cu have concentrated on the melting of the various monolayers and higher coverage phases. MFE studied the melting of the incommensurate monolayer and found that at the melting point ($\sim 250^\circ\text{C}$) the correlation length along both the [110] and the [001] decrease but, as the temperature is raised, the correlation length along the [001] increases. At still higher temperatures, the correlation length decreases to liquid-like lengths. They interpreted this result to mean that the chains of Pb atoms along the [110] were locked together with the solid phase and, as the chains disorder, considerable disorder is introduced along the [001]. Our crystallographic results suggest that steric constraints imposed by the large displacements along the [100] could account for these results.

ACKNOWLEDGMENTS

Some of this work was performed by S.B. while at the Exxon Research and Engineering Company. The authors would like to thank R. C. Hewitt, G. J. Hughes, and G. K. Sorenson for their assistance and to I. K. Robinson for his helpful comments. Some of the work described here was performed at Stanford Synchrotron Radiation Laboratory (SSRL), which is supported by the U.S. Department of Energy (Office of Basic Energy Sciences, Office of Energy Research), and by the National Institute of Health (Biotechnology Resource Program, Division of Research Resources).

¹J. Henion and G. E. Rhead, *Surf. Sci.* **29**, 20 (1972).

²W. C. Marra, P. H. Fuoss, and P. E. Eisenberger, *Phys. Rev. Lett.* **49**, 1169 (1982).

³S. Brennan, P. H. Fuoss, and P. Eisenberger, in *The Structure of Surfaces*, edited by M. A. Van Hove and S. Y. Tong (Springer-Verlag, Berlin, 1985), p. 421.

⁴S. Brennan and P. Eisenberger, *Nucl. Instrum. Methods* **222**, 164 (1984).

⁵G. H. Vineyard, *Phys. Rev. B* **26**, 4146 (1982).

⁶S. Dietrich and H. Wagner, *Phys. Rev. Lett.* **51**, 1469 (1983).

⁷I. K. Robinson, P. H. Fuoss, J. B. Stark, and P. A. Bennett (unpublished).

⁸We adopt the notation that the three-dimensional peak (nm) is expressed for the two-dimensional structure as (nm).

⁹W. C. Marra, Ph.D. thesis, Stevens Institute of Technology, 1981.

¹⁰R. W. James, *The Optical Principles of the Diffraction of X-Rays* (Ox Bow, Woodbridge, Conn., 1982).

¹¹*International Tables of X-Ray Crystallography*, edited by J. A. Ibers and W. C. Hamilton (Kynoch, Birmingham, 1974), Vol. IV, Table 3.3.1B.

¹²W. C. Hamilton, *Acta Crystallogr.* **18**, 502 (1965).

¹³C. Binns and C. Norris, *Surf. Sci.* **115**, 395 (1982).

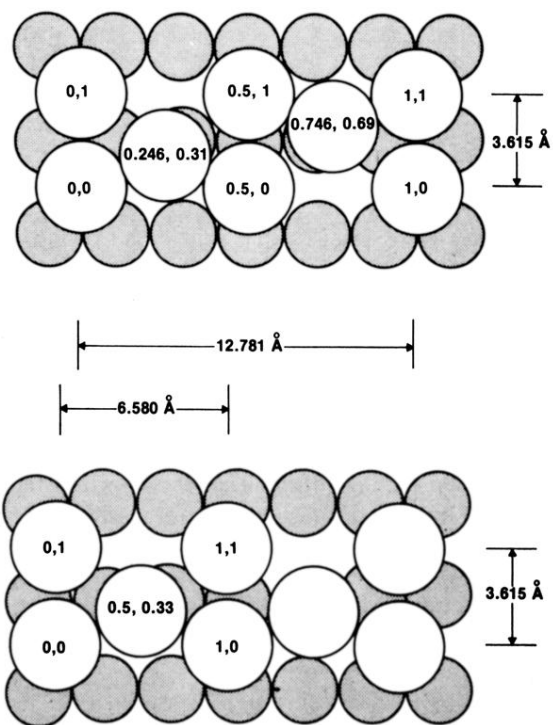


FIG. 3. The calculated structures of (a) the commensurate phase and (b) the incommensurate phase.